New Carbon Materials, 2023, 38(5): 976 - 988

Supporting Information

Highly efficient Co—N—C electrocatalysts with a porous structure for the oxygen reduction reaction

Xinfu He [a, b], Liaobo Chang [a], Pengfei Han [a], Keke Li [a], Hongju Wu [a], Yong Tang [a], Peng Wang [a], Yating Zhang [a, b, *], Anning Zhou [a, b]

[a] School of Chemistry and Chemical Engineering, Xi'an University of Science and Technology, Xi'an, 710054, China

[b] Key Laboratory of Coal Resources Exploration and Comprehensive Utilization, Ministry of Natural Resource, Xi'an, 710021, China

Corresponding author: Prof. Dr. Yating Zhang, School of Chemistry and Chemical Engineering, Xi'an University of Science and Technology, No.58 Yanta Road, Xi'an 710054, China. E-mail: isyating@163.com

1. Characterization of material

The synthesized catalysts were subjected to X-ray diffraction (XRD) patterns using a Rigaku MiniFlex-600 diffractometer with Cu Kα radiation (λ=0.1543 nm) at 40 kV, 30 mA at room temperature. The structure and morphology of the catalysts were determined through scanning electron microscopy (SEM, FEI Sirion 200), transmission electron microscopy (TEM, JEOL JEM-2100F), and high-resolution TEM (HRTEM, JEM-2100F). Elemental-mapping analysis were measured by energy-dispersive X-ray spectroscopy (EDS) equipped on FEI Sirion 200 SEM. Raman spectra were recorded on a Renishaw inVia Reflex spectrometer with 532 nm laser excitation. X-ray photoelectron spectroscopy (XPS) analysis of samples was carried out on a ThermoFisher Scientific K-Alpha instrument with a base pressure of 2×10^{-9} mbar. The specific surface area and corresponding pore size distribution curves of the catalysts were measured from the Brunauer-Emmett-Teller (BET) and Barrett-Joyner-Halenda (BJH) analysis of desorption data recorded at 77 K using a Quantachrome Autosorb-iQ3 adsorption instrument. The contact angles of catalysts were measured using a JC2000DM contact angle meter (Beijing Zhongyi Kexin Technology Co., Ltd).

2. Electrochemical measurements

All electrochemical experiments were implemented employing a three-electrode system on a Pine electrochemical workstation (Wave driver 20) outfitted with Pine Modulated Speed Rotator (model AFMSRCE) under ambient temperature. A

platinum wire and an Ag/AgCl (3 M KCl) electrode were used as the counter electrode and reference electrode, respectively. The glassy carbon rotating disk electrode (RDE) or glassy carbon rotating ring disk electrode (RRDE) modified with the prepared electrocatalysts served as working electrode. In terms of the preparation of the working electrode, 4.0 mg of the prepared catalyst was added to a mixed solution of 0.1 mL of 5.0% Nafion solution and 0.9 mL of deionized water. The obtained catalyst ink was sonicated for 1 h, and 10 μL of the solution was subsequently dropcast onto the freshly polished glassy carbon electrode (5 mm in diameter) and then dried naturally.

Before the electrochemical measurement, N_2 or O_2 was flowed into the KOH solution for 30 min to guarantee that it was saturated with N_2 or O_2, and the catalyst was activated by multiple cyclic voltammetry (CV) cycles until it generated a stable CV curve. The CV curves were recorded between −1.0 V to 0.2 V (vs. Ag/AgCl) and the chronoamperometry (CA) analysis were performed at 0.6 V with a scanning speed of 50 mV s^{-1}. The linear sweep voltammetry (LSV) measurements were conducted from 0.2 V to −1.0 V (vs Ag/AgCl) with a scan rate of 10 mV s^{-1} at rotation speeds range from 400 to 2500 rpm.

All the measured potentials in this work were referenced to the reversible hydrogen electrode (RHE) using the Nernst equation of $E_{[RHE]}=E_{[Ag/AgCl]}+0.197+0.059pH$. The number of electrons transferred per oxygen

molecule (n) during the ORR was calculated according to the Koutecky-Levich (K-L) equation:

$$\frac{1}{J}=\frac{1}{J_k}+\frac{1}{J_L}=\frac{1}{J_k}+\frac{1}{0.2nFc_O D_O^{2/3} v^{-1/6}\omega^{1/2}}$$

where J, J_K, and J_L are current density, kinetic-limiting current density, and diffusion-limiting current density, respectively; F represents Faraday constant (F=96485 C mol^{-1}); c_O refers to the bulk concentration of O_2 (1.2×10^{-6} mol cm^{-3}); D_O is the diffusion coefficient of O_2 in 0.1 M KOH at room temperature (1.9×10^{-5} cm^2 s^{-1}); v refers to the kinematic viscosity (0.01 cm^2 s^{-1}); ω corresponds to the rotational speed of the electrode in rpm.

The RRDE test was conducted via LSV from 0.2 V to −1.0 V (vs. Ag/AgCl) with a scanning speed of 10 mV s^{-1} at 1600 rpm, and the ring electrode potential was maintained at 1.3 V versus RHE. The number of transferred electrons and the yield of H_2O_2 were counted using the following equations:

$$n=\frac{4I_D}{I_D+I_R/N}$$

$$H_2O_2\%=\frac{200\,I_R/N}{I_D+I_R/N}$$

where I_R and I_D represent the ring current and disk current, respectively, and N means the current collection efficiency (0.40) of the Pt ring.

3.Experimental section

3.1 Preparation of polystyrene (PS) spheres

The styrene raw material was washed with 10wt.% NaOH solution and ultrapure water to remove the polymerization inhibitor and other impurities, followed by vacuum distillation to obtain refined styrene monomer. Of the refined styrene monomer 50 mL, 200 mL of water, and 0.9 g of hexadecyl trimethyl ammonium bromide (CTAB) were added to a 500 mL round-bottom three-necked flask. After stirring for 30 min, 40 mL of an aqueous solution containing 0.3 g $K_2S_2O_8$ (AR) was added to the above emulsion as an initiator. The polymerization reaction lasted for 24 h at 70 ^oC with stirring under N_2 atmosphere. After the milk-like product was cooled down, the monodispersed PS suspension was obtained. Vacuum filtration was used to obtain an ordered PS template.

3.2 Synthesis of ZIF@PS-x

0.35 g of the prepared PS spheres were fully ground and dispersed in 90 mL of methanol containing 1 g of polyvinyl pyrrolidone (PVP). After ultrasonic dispersion and vigorous agitation for 3 h, 8.0 g of $Zn(NO_3)_2·6H_2O$ (ZNH) and 100 mg of $Co(NO_3)_2·6H_2O$ (CNH) were dissolved in the mixed solution and stirred for another 0.5 h. Then, 8.0 g of 2-methylimidazole (2-MI, *m*(ZNH)/*m*(2-MI)=1) dissolved in 100 mL of methanol was quickly added into the above solution followed by vigorous stirring for 4 h. Finally, the ZIF@PS-1 precursors were collected by centrifugation, washed with methanol for several times, and dried at 60 °C overnight. The same

procedures were used to synthesize ZIF@PS-2, ZIF@PS-3, ZIF@PS-4, and ZIF@PS-5 with exception that the mass ratio of *m*(ZNH)/*m*(2-MI) was adjusted to 0.6, 0.5, 0.33, 0.25, respectively.

3.3 Synthesis of Co-NHCP-x

The derived ZIF@PS-1, ZIF@PS-2, ZIF@PS-3, ZIF@PS-4, and ZIF@PS-5 particles were heated to 900 °C at a heating rate of 5 ^{o}C min^{-1} under N_2 atmosphere and stayed for 5 h for carbonization. The desired composites Co-NHCP-1, Co-NHCP-2, Co-NHCP-3, Co-NHCP-4, and Co-NHCP-5 were obtained after natural cooling these particles to room temperature.

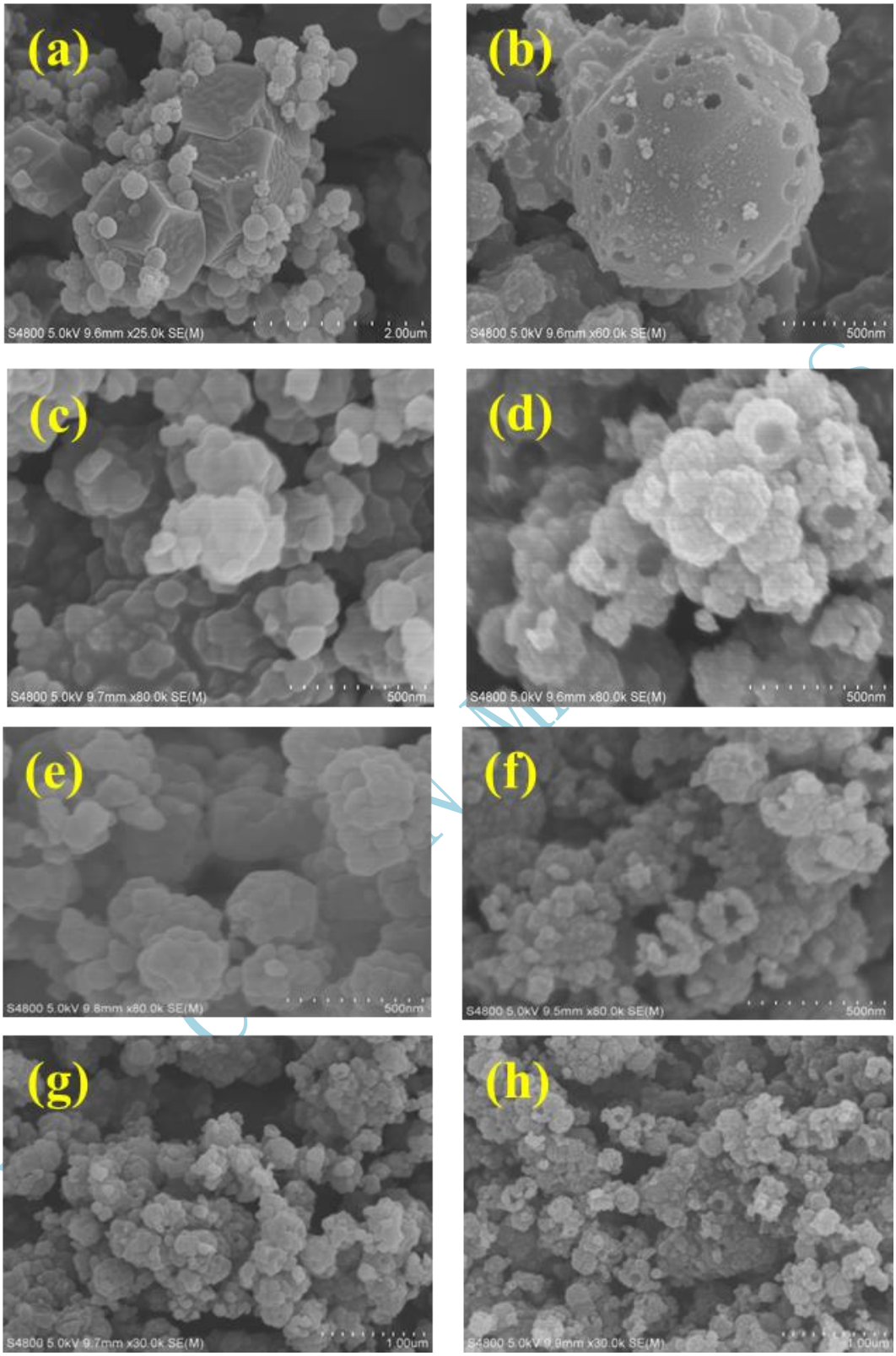

Fig. S1 SEM images of (a) ZIF@PS-1; (b) Co-NHCP-1; (c) ZIF@PS-3; (d) Co-NHCP-3; (e) ZIF@PS-4; (f) Co-NHCP-4; (g) ZIF@PS-5 and (h) Co-NHCP-5.

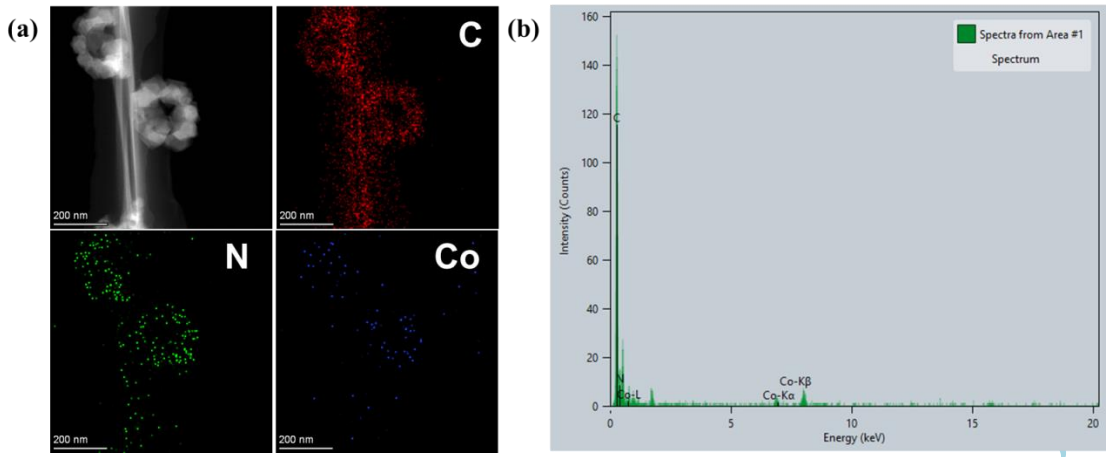

Fig. S2 (a) EDS surface scanning elemental mapping images of Co-NHCP-2; (b) EDS line scanning elemental mapping image of the Co-NHCP-2.

Table S1 Summary of the specific surface area, pore volume and average pore size of catalysts.

Catalysts	BET surface area (m^2 g^{-1})	Pore volume (cm^3 g^{-1})	Average pore size (nm)
Co-NHCP-1	383.92	0.27	3.48
Co-NHCP-2	1817.24	1.80	3.48
Co-NHCP-3	549.84	0.45	3.10

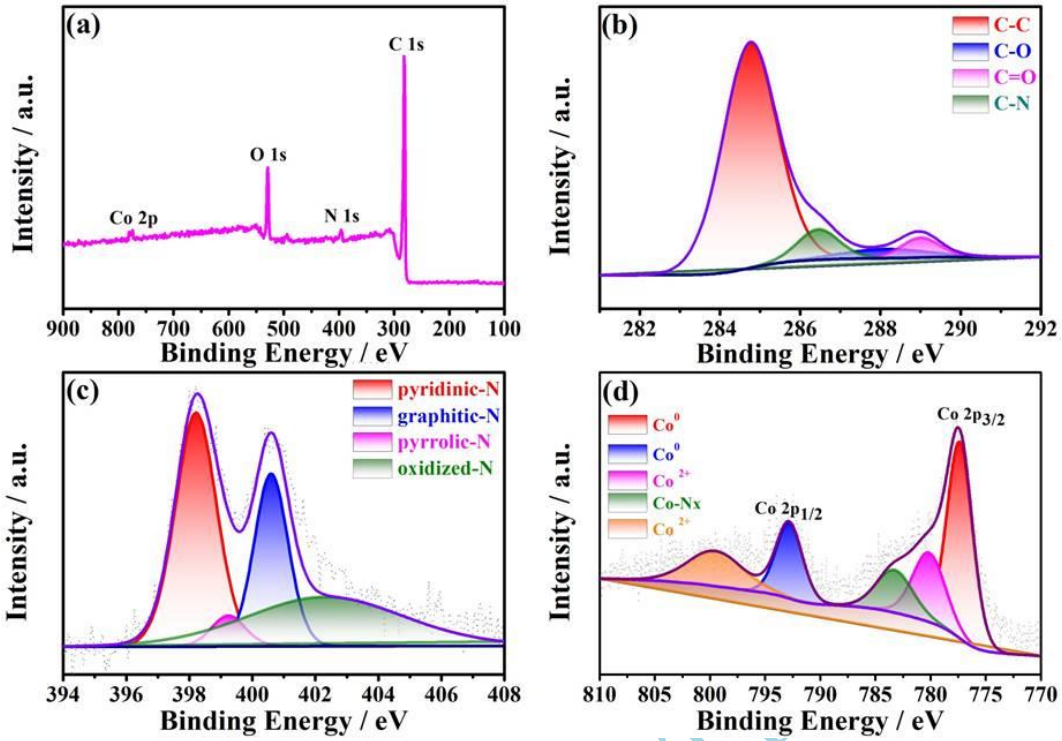

Fig. S3 High resolution XPS spectra of Co-NHCP-1: (a) survey; (b) C 1s; (c) N 1s and (d) Co 2p.

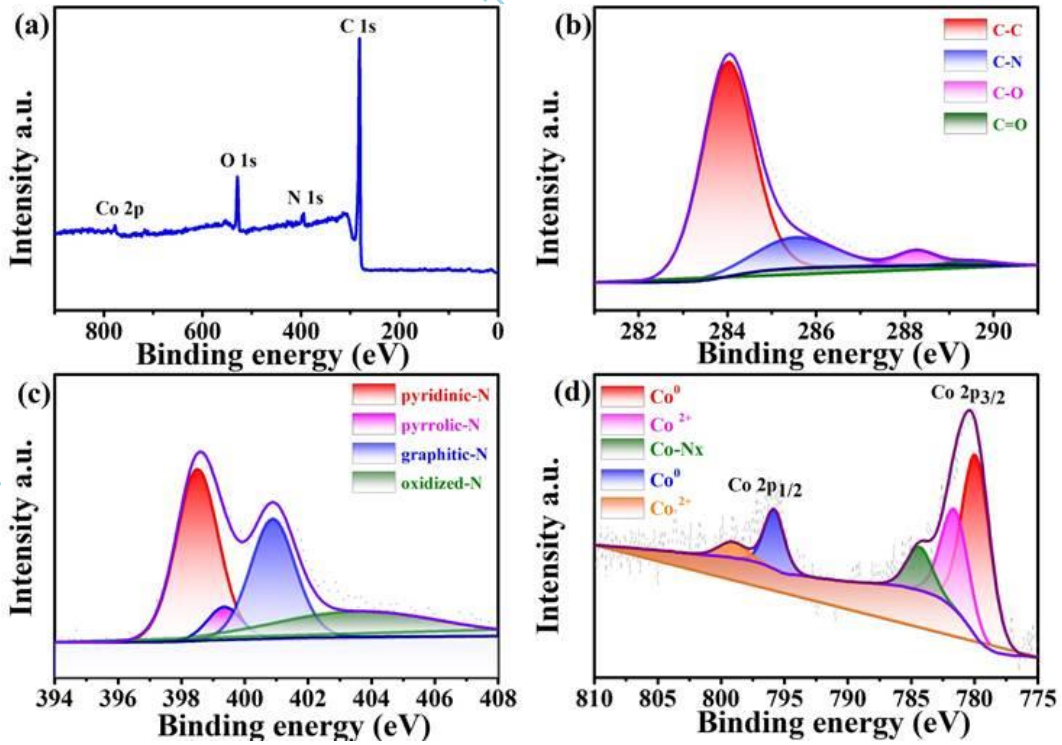

Fig. S4 High resolution XPS spectra of Co-NHCP-3: (a) survey; (b) C 1s; (c) N 1s and (d) Co 2p.

Table S2 Elemental analysis of catalysts.

Catalysts	Content (at.%)			
	C	N	O	Co
Co-NHCP-1	87.36	3.77	8.35	0.52
Co-NHCP-2	90.74	5.28	3.46	0.52
Co-NHCP-3	89.10	5.04	5.39	0.47

Table S3 N 1s peak fitting results of catalysts.

Catalysts	Pyridinic-N (%)	Pyrrolic-N (%)	Graphitic-N (%)	oxidized-N (%)
Co-NHCP-1	36.73	5.30	27.20	29.77
Co-NHCP-2	37.98	15.45	39.20	7.37
Co-NHCP-3	37.93	6.30	30.89	24.88

Table S4 Co-N_x peak area as a percentage of Co 2p peak area.

Catalysts	Co-NHCP-1 (%)	Co-NHCP-2 (%)	Co-NHCP-3 (%)
Co-Nx	12.47	16.53	9.67

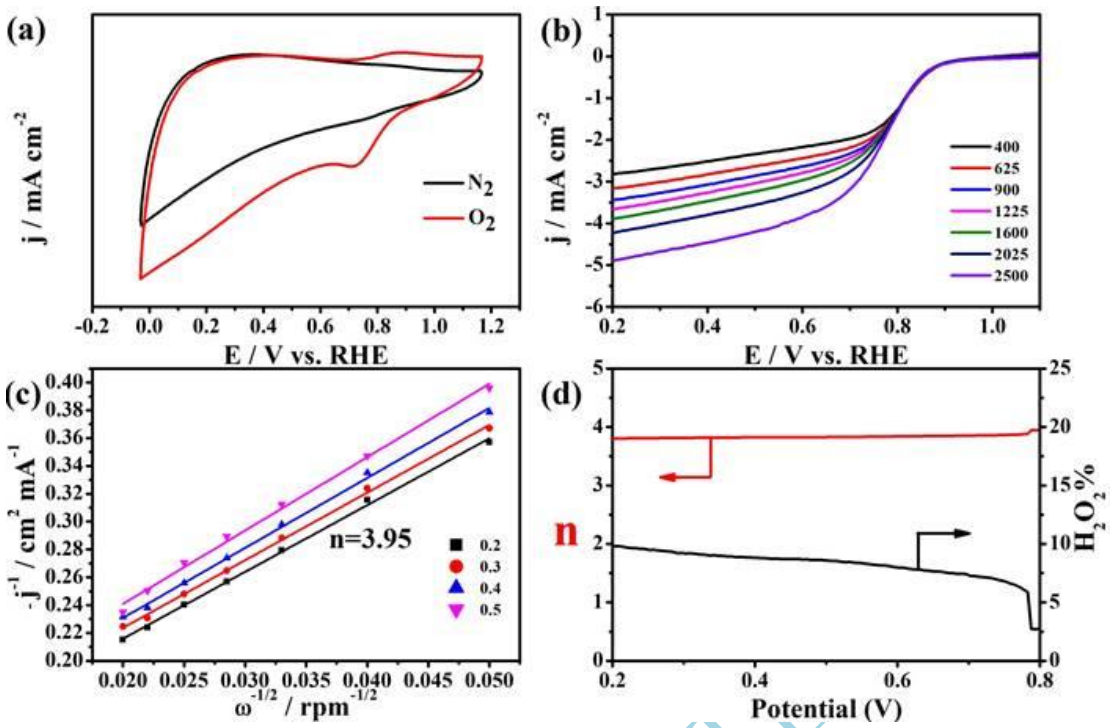

Fig. S5 (a) CV curves of Co-NHCP-1 on glassy carbon electrode in O_2 or N_2-saturated 0.1 M KOH; (b) LSV curves of Co-NHCP-1 in 0.1 M O_2-saturated KOH electrolyte at rotational speed ranging from 400 to 2500 rpm with scanning rate of 10 mV s^{-1}; (c) Corresponding Kouteck-Levich plots derived from the RDE data; (d) The number of transferred electrons (*n*) and yield of H_2O_2 calculated from the RRDE results.

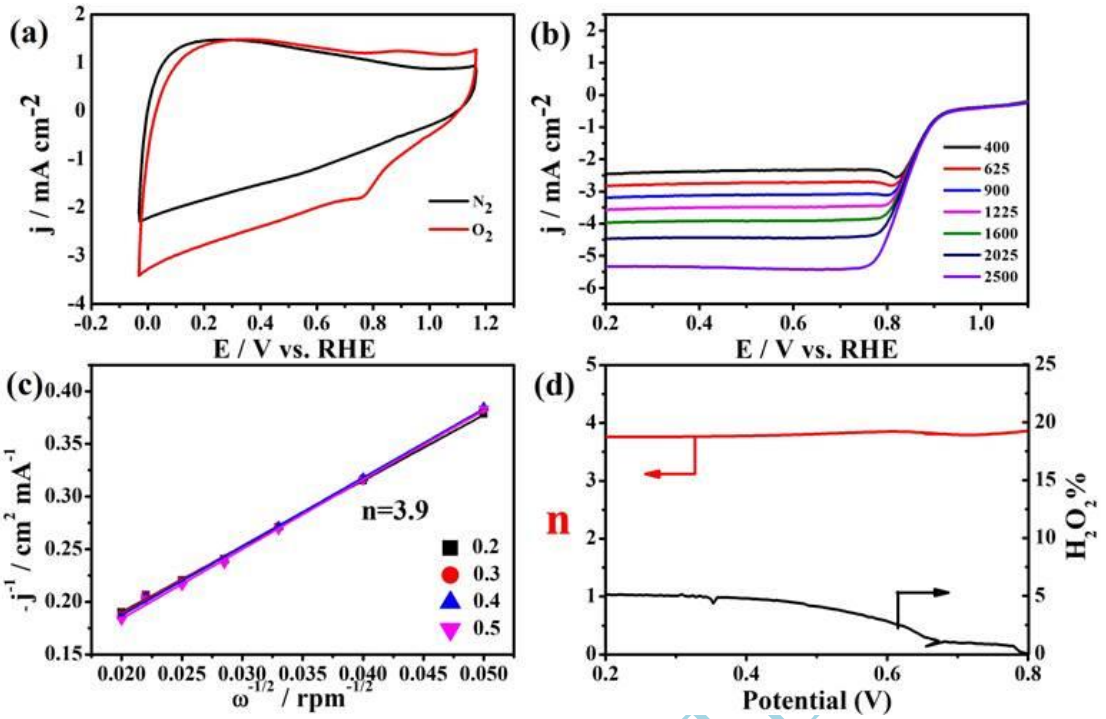

Fig. S6 (a) CV curves of Co-NHCP-3 on glassy carbon electrode in O_2 or N_2-saturated 0.1 M KOH; (b) LSV curves of Co-NHCP-3 in 0.1 M O_2-saturated KOH electrolyte at rotational speed ranging from 400 to 2500 rpm with scanning rate of 10 mV s^{-1}; (c) Corresponding Kouteck-Levich plots derived from the RDE data; (d) The number of transferred electrons (*n*) and yield of H_2O_2 calculated from the RRDE results.

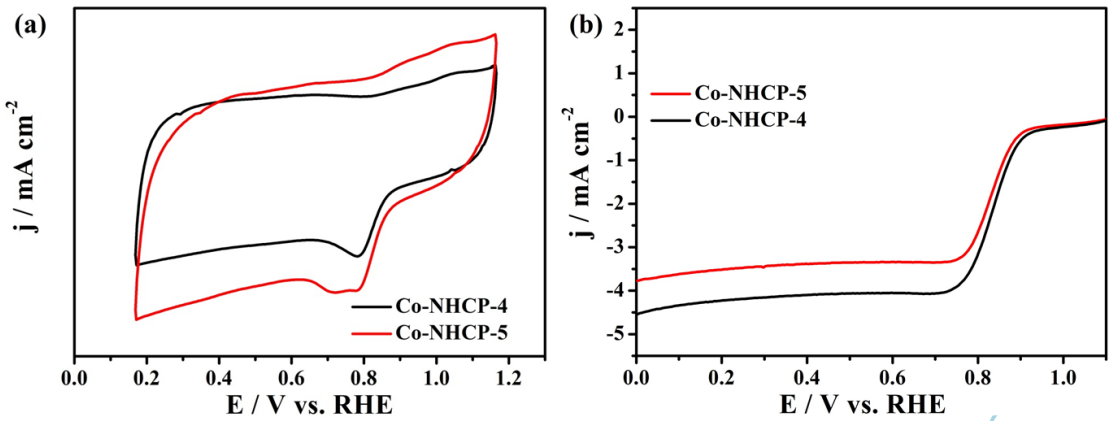

Fig. S7 (a) LSV curves of Co-NHCP-4 and Co-NHCP-5 in 0.1 M O_2-saturated KOH electrolyte at rotational speed 1600 rpm with scanning rate of 10 mV s^{-1}; (b) CV curves of Co-NHCP-4 and Co-NHCP-5 on glassy carbon electrode in O_2 -saturated 0.1 M KOH.

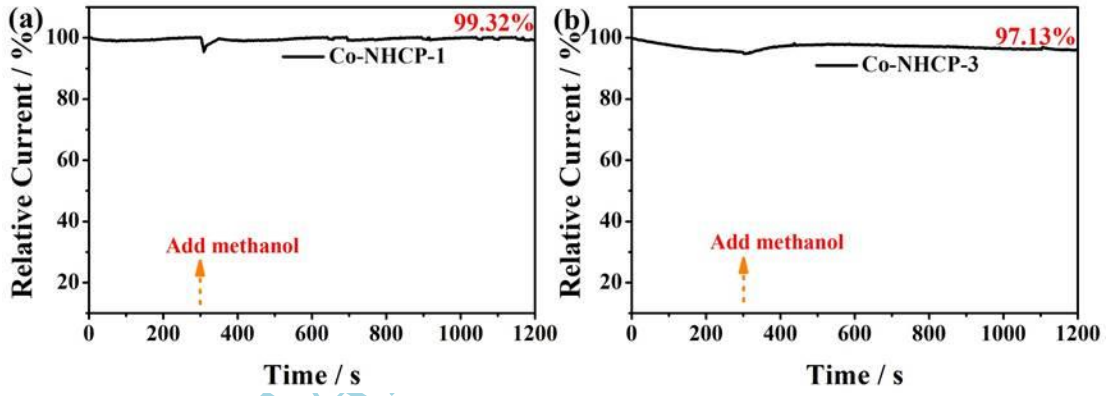

Fig. S8 Chronoamperometric responses of (a) Co-NHCP-1 and (b) Co-NHCP-3 by injecting 2wt% of methanol at 300 s.

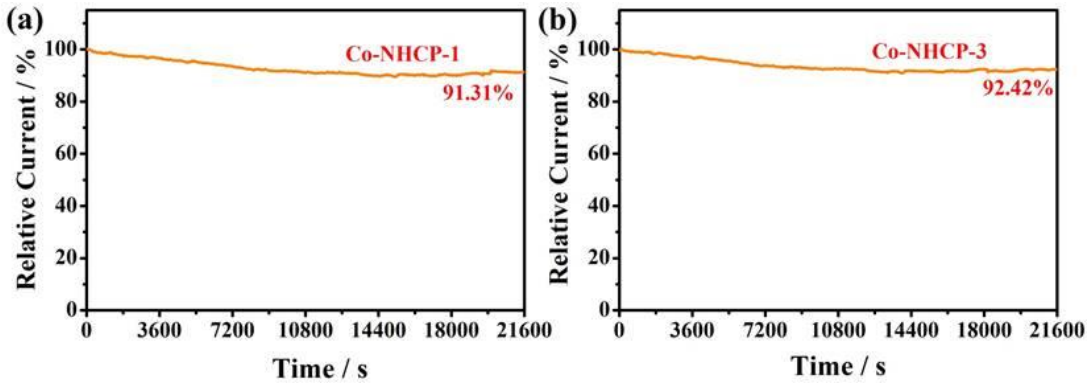

Fig. S9 (a) Chronoamperometric responses of (a) Co-NHCP-1 and (b) Co-NHCP-3 obtained under O_2-saturated 0.1 M KOH electrolyte at 1600 rpm.

Table S5 Comparison of ORR performances under alkaline conditions for this work with other reported benchmark catalyst.

Electrocatalyst	Catalyst loading (mg cm^{-2})	Electrolyte	E_{onset} (V vs. RHE)	$E_{1/2}$ (V vs. RHE)	Limited current density (mA cm^{-2})	Reference
Co-NHCP-2	0.4	0.1 M KOH	0.96	0.84	5.5	This work
Pt/C	0.2	0.1 M KOH	0.95	0.82	5.0	This work
Co–Fe/NC-700	0.25	0.1 M KOH	0.97	0.854	5.8	Small, 2019, 15(13): 1805324.
FeS/Fe3C@NS-C	0.1156	0.1 M KOH	1.03	0.78	6.83	ACS Appl. Mater. Inter., 2020, 12(40): 44710-44719
Co-HNCS-0.2	0.1	0.1 M KOH	0.94	0.82	5.8	Chem. Eng. J., 2017, 330(15): 736-745.
Co- NOPC	0.6	0.1 M KOH	0.95	0.86	5.2	ChemSusChem, 2020, 13(4):741-748.
10Co-N@DCNF	0.1	0.1 M KOH	—	0.83	6.5	Angew. Chem. Int. Ed., 2020, 59: 6122.
Co_9S_8-HCT	0.204	0.1 M KOH	0.95	0.86	5.5	Chem. Eng. J., 2021, 418: 129365.
Co-N-mC	0.28	0.1 M KOH	0.940	0.851	4.7	Small, 2017, 13(3): 1602507.
Co,N-C900	0.24	0.1 M KOH	0.97	0.85	5.82	J. Mater. Chem. A, 2018, 35(6): 17067-17074.
Co@BNCNTs-900	—	0.1 M KOH	0.93	0.82	5.3	J. Mater. Chem. A, 2018, 6: 24071-24077.
L-CCNTs-Co-800	—	0.1 M KOH	0.90	0.84	5.1	Angew. Chem. Int. Ed., 2018, 130: 13371-13375.
NG800	1.1	0.1 M KOH	0.88	0.76	4.0	J. Power Sources, 2019, 438: 227036.
N-hG	0.25	0.1 M KOH	0.91	0.833	5.0	Carbon, 2020, 162(10): 66-73.
Co@N-CNTF-2	0.285	0.1 M KOH	0.91	0.81	5.0	J. Mater. Chem. A, 2019, 7: 3664-3672.
N-Co3O4@NC-2	1.0	0.1 M KOH	0.89	0.77	5.87	Adv. Funct. Mater., 2019, 29(33): 1902875.
Co-V-N/NC	0.486	0.1 M KOH	0.98	0.85	6.1	Carbon, 2020, 159: 16-24.
Co,N-CNC-800	0.3	0.1 M KOH	0.924	0.816	4.9	Int. J. Hydrogen Energ., 2020, 45: 6318-6327.
Co-N-Cs	—	0.1 M KOH	0.92	0.84	5.54	Adv. Funct. Mater., 2020, 30(10):1908945.

Co@N-HCCs@NG	0.4	0.1 M KOH	0.98	0.860	5.8	Carbon, 2021, 177: 344-356.